

Chapter 4

Multiscale Ice Fluidity in NO_x Photodesorption from Frozen Nitrate Solutions [†]

C. S. Boxe[¶], A. J. Colussi^{¶*}, M. R. Hoffmann[¶], D. Tan[§],
J. Mastromarino[§], A. T. Case[§], S. T. Sandholm[§], D. D. Davis[§]

[¶]W. M. Keck Laboratories, California Institute of Technology, Pasadena, CA 91125,

[§]School of Earth and Atmospheric Sciences, Georgia Institute of Technology, Atlanta,
GA 30332

This chapter has been published as a journal article.

[†]*Journal of Physical Chemistry A* (2003) **107**: 11409-11413.

IV-2

Abstract

The temperature programmed desorption of nitric oxide, NO, and nitrogen dioxide, NO₂, during the 302 nm photolysis of KNO₃-doped, spray-frozen ice layers was investigated using two-photon laser-induced NO_x fluorescence detection in the range $-35 \leq T/\text{°C} \leq 0$. Upon applying steady illumination, and a 0.67 °C min^{-1} heating ramp to frozen KNO₃ solutions, NO₂ begins to evolve at increasing rates, while NO emissions plateau soon after until, at $\sim -8 \text{ °C}$, both species surge abruptly. Although the primary photoproduct NO₂ avoids geminate recombination by escaping from a permeable molecular cage throughout, NO₂(g) levels are controlled by desorption from the outermost ice layers rather than by NO₃⁻ photolysis rates. The NO_x accumulated in the deeper layers bursts when the solid undergoes a sintering transition following the onset of surface melting at -10 °C . Since elementary photochemical events occur in a communal fluid phase of molecular dimensions at temperatures far below the KNO₃/H₂O eutectic ($T_{\text{eutectic}} = -2.88 \text{ °C}$), we infer that doped polycrystalline ice contains operationally distinguishable fluid phases of low dimensionality over various length scales and temperature ranges.

Introduction

The constant nitrate levels across the Antarctic ice shelf reflect remote atmospheric sources.¹ It has been long assumed that the composition of paleoatmospheres could be retrieved from polar nitrate records, were they preserved over geological periods.² There is now evidence, however, that the topmost nitrate deposits undergo post-depositional photochemical processing leading to NO_x reemissions.³⁻⁶

Nitrate is a major chromophore in polar ice and snow.⁷ Its solar photolysis via excitation of a weak ($\epsilon_{\text{max}} = 7.14 \text{ M}^{-1} \text{ cm}^{-1}$) transition peaking at 302 nm yields nitrogen dioxide, NO₂, and nitrite, NO₂⁻, as primary photoproducts:^{8,9}



These processes are deemed to underlie the excessive NO_x levels found over snow and ice at high latitudes during early spring.^{4,7} The reactive O- and OH-radicals generated in reactions 2 and 3 may induce the chemical transformation of other contaminants.

We recently investigated the photolysis of spray-frozen aqueous millimolar nitrate solutions,^{8,9} and found that the steady-state NO₂⁻ concentrations ultimately reached in the solid, as well as the NO₂ fluxes released into the gas-phase, were independent of the thickness of submillimeter ice layers. Thus, only the NO₂ generated in the outermost strata of homogeneously irradiated ice deposits can escape into the gas-phase. Moreover, the monotonic temperature dependence of ϕ_3 about the freezing point over the range 238

IV-4

- 294 K, and the inhibiting effect of formate on NO_2^- losses in non-geminate radical reactions, revealed that the elementary photochemical processes 1-3 actually take place in a quasi-liquid medium down to about -35 °C.^{8,9}

These observations point to the plasticity of ice aggregates at environmental temperatures, both at the dimensions probed by molecular events such as reaction 3,¹⁰ and at the mesoscale features that determine the porosity and diffusivity of polycrystalline ices responsible for NO_2 emissions.¹¹⁻¹⁶ The nature, extent and rates of photochemical processes in snow and ice, and their impact on the composition of the overlying atmosphere are expected, therefore, to depend on the interplay of thermal and radiative effects. In this report we explore further these fundamental issues by monitoring NO_x emissions in real time from steadily illuminated ($\lambda \geq 300$ nm) nitrate-doped ice layers subjected to a linear temperature ramp.

Experimental Section

A schematic representation of the experimental setup is shown in Fig. 4.1. Uniform nitrate-doped ice layers were produced by spraying precooled KNO_3 solutions (2 μM , 10, and 50 mM, Fisher Scientific) onto the surface of a cold finger (CF in Fig. 4.2, exposed area $A = 304 \text{ cm}^2$). The ice-laden CF was then enclosed in a quartz sheath (QS) provided with a ground joint, and the array placed along the axis of a reflective cylindrical chamber. Compact-equivalent ice layers varied from 3.5 cm^3 to 9.0 cm^3 in volume, and from 110 μm to 284 μm in thickness, respectively.¹⁷ The temperature of the ice deposits was controlled by circulating refrigerated fluid from a cryogenic unit through the coldfinger. In all experiments, temperature was increased at $0.67 \text{ }^\circ\text{C min}^{-1}$ from ~ -40 $^\circ\text{C}$ to 0 $^\circ\text{C}$, while exposing the ice deposits to the combined output of three, 5" long Hg

Pen-Ray UV lamps emitting at $\lambda = 313 \pm 20$ nm. The available actinic flux: 1.3×10^{15} photons $\text{cm}^{-2} \text{ s}^{-1} \sim 0.3$ sun equivalents, was determined by ferrioxalate actinometry.¹⁸ Lamp stability was monitored by a photocell (UDT Sensors, model PIN UV 100L) attached to the top of the chamber. A continuous flow of $5 \text{ L N}_2 \text{ min}^{-1}$ swept the photogenerated NO_x species into the detection zone within 3.9 s (Fig. 4.1).

The trace NO_x levels present in the carrier gas effluent were detected by two-photon induced fluorescence.¹⁹ In this approach, NO is detected by exciting the $\text{NO X}^2\text{II}$ ground-state to the $\text{D}^2\Sigma$ excited state via the $\text{A}^2\Sigma$ state using (226 nm + 1097 nm) laser pulses (Fig. 4.1). The resulting $\text{D}^2\Sigma \rightarrow \text{X}^2\text{II}$ fluorescence is monitored at 183 nm. NO_2 is detected by prior photolysis into NO at 355 nm. NO_2 concentrations are obtained from the difference between the NO fluorescence signals obtained with the 355 nm beam on and off.¹⁹

Results and Discussion

The NO_2 concentrations exiting the photochemical reactor during the photolysis of frozen 50 mM, 10 mM and 2 μM aqueous nitrate solutions under a linear temperature ramp are shown in Figures 4.3-4.5. NO measurements in the 50 mM nitrate experiments are shown in Fig. 4.3a. Under steady flow conditions, gas-phase NO_x concentrations are directly proportional to NO_x desorption rates. It is apparent that: 1) NO_2 is released from the solid at increasingly faster rates, while the smaller NO emission rates approach a temperature-independent value after a detectable delay,^{3,20} 2) NO_x emission rates from ice doped with mM nitrate levels abruptly surge and peak out above -8°C and, 3) NO_2 emissions from frozen 2 μM nitrate monotonically approach melting instead. We estimate that the ~ 500 pptv NO_2 levels above illuminated frozen 50 mM KNO_3 solutions

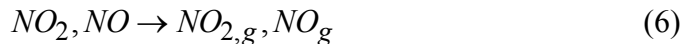
IV-6

at about -20°C (Figure 4.3a) correspond to $F_{\text{NO}_2} \sim 6 \times 10^{-15} \text{ mol cm}^{-2} \text{ s}^{-1}$. This figure, after being scaled by the relative actinic fluxes, is within a factor of 2 of the F_{NO_2} values previously measured in this setup.⁸

The intrinsic temperature dependences of NO_2 and NO_2^- photoproduction rates in polycrystalline ice had been previously determined in experiments performed under isothermal conditions: $R_2(T) \propto \exp(-5037/T)$,⁸ and $R_3(T) \propto \exp(-2402/T)$.⁹ The fact that NO_2^- concentrations under continuous photolysis ultimately reach steady-state in the absence of formate were ascribed to the occurrence of secondary dark reactions, reaction 4, and, possibly, to secondary photolysis, reaction 5:^{9,21}



In isothermal experiments, after an initial induction period in which photoproducts within the ice matrix reach either equilibrium or steady-state regimes—depending on whether desorption rates are slower or faster than production rates, respectively—the net emission rates of gas-phase species become photon-controlled. In contrast, during transient experiments, such as the present ones, emission rates may be overtaken and lag behind photon absorption rates as the temperature increases. The apparent rate constants for the desorption of photogenerated species, k_6 , from a morphologically stable solid:



are expected to increase exponentially with temperature. The removal of NO_x from the illuminated region by the carrier gas, reaction 7:



proceeds in this case with: $k_7 = 1/(3.9 \text{ s}) = 0.26 \text{ s}^{-1}$.

To test whether the instantaneous gas-phase NO₂ levels were controlled by photoproduction, reaction 2, or desorption, reaction 6, under present conditions, we overlaid (see Figure 4.3b) the known temperature dependence of reaction 2, R₂(T),⁸ on the NO₂ thermogram of Figure 4.3a. If the gas-phase NO₂ signals observed in present experiments were determined by the rate of reaction 2, after an initial induction period in which concentrations profiles within the ice matrix become stationary, they would track the R₂(T) dependence. It is apparent in Figure 4.3b that this condition is only realized below -27 °C. At higher temperatures, NO₂ increases at a lower rate than predicted by R₂(T), i.e., NO₂ release rates into the gas-phase become partially controlled by desorption. This condition would eventually develop and hold if the difference of apparent activation energies: E₆ - E₂ < 0. As a consequence, some of the photogenerated NO₂ is transiently retained in the solid above -27 °C under present conditions, where it may be further processed via photolysis, reaction 8:



or by reaction with OH-radicals, the reverse of reaction 2. The fact that NO₂ bursts at about -8 °C —and peaks out at about -4 °C— is consistent with the release of a NO₂ backlog. Since NO levels surge simultaneously, as shown in Figure 4.3a, this phenomenon seems to be associated with a metamorphic transition of the solid rather

than with the acceleration of elementary photoreaction rates. Thus, our system kinetically behaves as if k_6 for *both* species significantly jumped in less than a minute at about -8°C , due to the densification of the solid. Below, we analyze the implications of these results on the fluidity of ice at the molecular and mesoscopic scales.

The monotonic increase of quantum yields ϕ_2 and ϕ_3 with temperature found in isothermal experiments over the range $238 \leq T/\text{K} \leq 268$ is consistent with the enhanced probability of escape of primary photochemical fragments from a liquid-like cage in ice as well as in water.^{8-10,22} The fact that HCOO^- , an efficient OH-radical scavenger,²³ significantly increases the apparent quantum yield of NO_2^- formation, ϕ_3 , reflects a supramolecular communal fluid reaction medium in which the scavenger statistically competes with nitrite for OH-radicals.⁹ The emerging picture is that elementary photochemical processes, reactions 1-5, take place in an extended fluid layer at least a few nanometers thick. The temperature dependence of molecular diffusivity in such a layer is similar, but not identical to that of bulk supercooled water.⁹

Most solutes, including nitrates, are too large to be molecularly incorporated within the ice lattice and are rejected upon freezing.²⁴⁻³⁰ The extent of interfacial ion separation upon freezing dilute solutions depends on freezing rates and solute concentration.³¹ The associated polarization decays soon after, however.³² In our experiments, the fast cooling and freezing upon impact of spray droplets on a cold surface likely generates heterogeneous ice deposits in which $\text{KNO}_3(\text{s})$ or $\text{KNO}_3/\text{H}_2\text{O}$ solutions, depending on temperature, are interspersed with ice layers. From a thermodynamic point of view, KNO_3 as a photolyte can reside in macroscopic aqueous solutions along the liquidus curve down to the eutectic temperature: $T = -2.88^{\circ}\text{C}$, and as

a macroscopic $\text{KNO}_3(\text{s})$ phase below. What is the nature of the fluid phases in which nitrate photolysis is taking place down to at least $-35\text{ }^\circ\text{C}$? Several mechanisms are responsible for the existence of liquid at temperatures within the solid region of the bulk phase diagram. There is substantial evidence that solute impurities are concentrated in ‘subeutectic’ fluid phases filling the veins and nodes of polycrystalline ice. These phases arise from a combination of colligative and interfacial curvature effects.³³ Thus, for example, ^1H and ^{23}Na NMR signals in ‘frozen’ NaCl aqueous solutions remain significantly narrower than in the solid down to $-45\text{ }^\circ\text{C}$ (cf. the eutectic point at $-21\text{ }^\circ\text{C}$).^{34,35}

Interfacial subeutectic films do not violate Gibbs’ phase rule because the explicit consideration of such phases requires introducing an additional intensive variable, viz. the interfacial tension, over temperature and external pressure that allows for an extra degree of freedom. Therefore, the coexistence of three bulk phases, in this case ice, $\text{KNO}_3(\text{s})$ and a 1.28 M KNO_3 solution, at the eutectic does not necessarily define an invariant point in a condensed system, unless films and surfaces are ignored. Furthermore, the composition of the subeutectic interfacial solution need not be uniform across its thickness, and could involve H^+ and OH^- as well as solute ions, unless electric fields across the interface were ignored.^{36,37} Subeutectic solutions may be either encapsulated by ice or lie at its interfaces. Thus, a subeutectic fluid film of decreasing viscosity as a reaction medium could account for the positive temperature dependences of ϕ_2 and ϕ_3 in ice.

Snow and polycrystalline ice kept at temperatures not far below melting would gradually develop into compact materials by sintering. The rates and mechanisms by

IV-10

which sintering occurs in ice aggregates are fairly well known.^{12,38} There is considerable empirical evidence that polycrystalline ice, in contrast with single ice crystals, becomes significantly softer above -10°C .^{38,39} Surface diffusion becomes the dominant mechanism above the onset of surface melting.^{12,39-41} Thus, metamorphic transformations in polycrystalline ice, such as the one invoked above to account for the bursting of NO_x at about -8°C , necessarily involve mesoscopic mass transfer. We argue that since liquid veins and triple junctions in ice owe their existence to the presence of diverse solutes at variable concentrations,^{24,33,42} *they can not account for a universal softening transition temperature.* In contrast, the inception of mass diffusion associated with surface melting, in which *all* ice/vapor interfaces are wetted by a liquid film of finite nanoscopic depth even in the absence of solutes, represents a general mechanism for temperature-dependent ice sintering at atmospheric pressures.^{15,16} Wetting arises from the intermediate Hamaker constant of water relative to the encompassing phases. The thickness of the wetting film is finite, however, due to relativistic retardation effects on van der Waals forces.^{40,43} Solutes presumably enhance wetting.⁴⁴

A recent infrared study of thin, uncontaminated ice films has supplied definitive evidence that the thickness of the quasi-liquid layer on exposed ice surfaces begins to exceed the limit of detection ($\sim 0.3\text{ nm}$) above -10°C ,⁴⁵ confirming the onset (although not the magnitude of the layer thickness) previously determined by AFM,⁴⁶ and early theoretical predictions.⁴¹ Therefore, our proposal that the simultaneous NO and NO_2 surges at about -8°C should be ascribed to the sudden availability of gas occluded within polycrystalline ice seems to be entirely compatible with previous empirical information, and with the predicted acceleration of sintering rates via surface diffusion

upon the premelting of pristine ice/vapor interfaces. Interstitial cavities will open up as water begins to diffuse through the liquid film from convex to concave regions,¹² until the liquid that bridges the receding convex features snap at threshold gaps.⁴⁷ The implicit requirement seems to be that KNO₃ subeutectics be confined to concave pockets. In this context, the monotonic evolution of NO₂ up to the melting point in the thermogram of the photolysis of 2 μM NO₃⁻ (Figure 4.5) is attributed to the fact that desorption remains faster than photogeneration at low photolyte concentrations, rather than to solute effects on surface premelting.⁴⁴

The remarkably constant NO levels before the sintering transition (Figure 4.3a) impose severe restrictions on the mechanism of formation. They seem to exclude condensed-phase photochemical control, reaction 5, for otherwise (cf. the evolution of NO₂ in the same experiment) NO signals would display a significant temperature dependence. In contrast, the NO/NO₂ ratio is largest at the lower temperatures, such as those prevalent in the South Pole⁴ and drops steadily. Should NO derive from the secondary photolysis of NO₂, reaction 8, it would eventually track NO₂ signals. In our previous study on nitrate photolysis we noticed that, whereas NO₂⁻ formation rates increase with temperature, NO₂⁻ losses via secondary reactions become slower, a fact that we attributed to the dilution effect associated with a thicker fluid phase.⁹ The net result is that steady-state NO₂⁻ concentrations increase with temperature and, therefore, the rate of reaction 5 would follow a similar trend. However, if NO were formed via a secondary dark reaction of NO₂⁻ its levels would reflect the combined temperature dependences of NO₂⁻ and the extent of secondary pathways. Further work is required to clarify this issue.

Captions to Figures

Figure 4.1: Schematic diagram of the experimental setup. 1. Photolysis cell (see Figure 4.2); 2. Reflective reaction chamber; 3. Pen-Ray UV lamps emitting at $\lambda_{\max} \approx 313$ nm; 4. Circulating cryostat; 5. Flow cell; 6. N₂ carrier gas.

Figure 4.2: The reaction cell. CF: Cold finger; QS: Quartz sheath.

Figure 4.3a: O: NO₂; ◇: NO, released from irradiated 50 mM nitrate-doped polycrystalline ice vs. temperature.

Figure 4.3b: O: NO₂ data from Figure 3a; Solid line: (scaled) primary photoproduction rates $R_2 \propto \exp(-5037/T)$.⁸

Figure 4.4: O: NO₂ released from irradiated 10 mM nitrate-doped polycrystalline ice vs. temperature

Figure 4.5: O: NO₂ released from irradiated 2μM nitrate-doped polycrystalline ice vs. temperature.

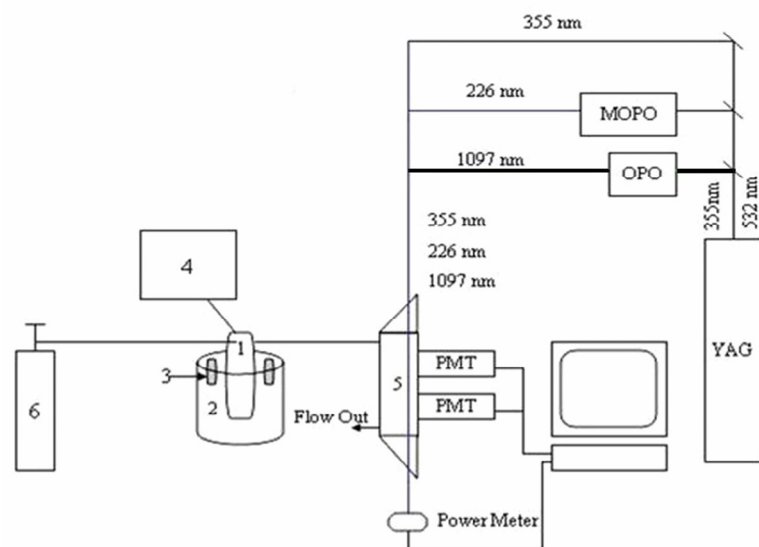


Figure 4.1

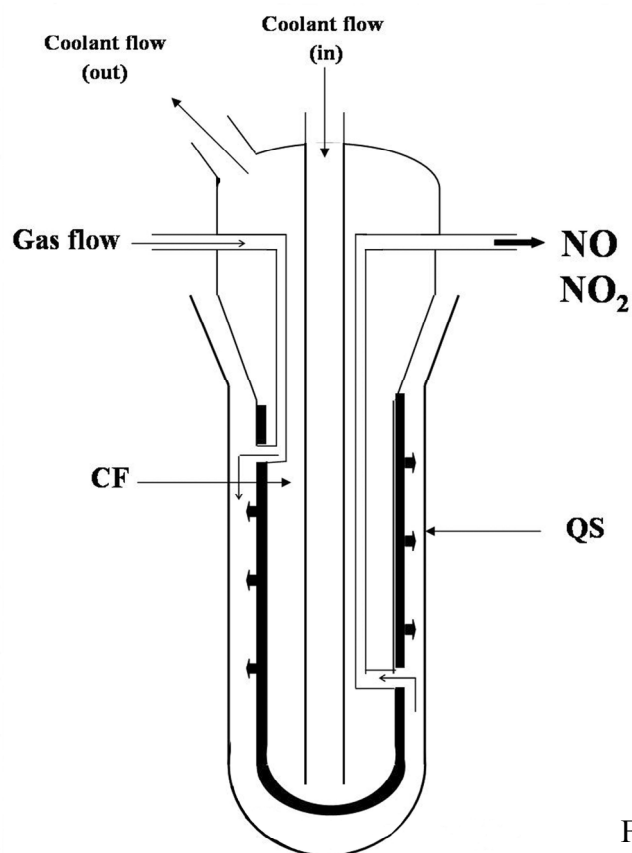


Figure 4.2

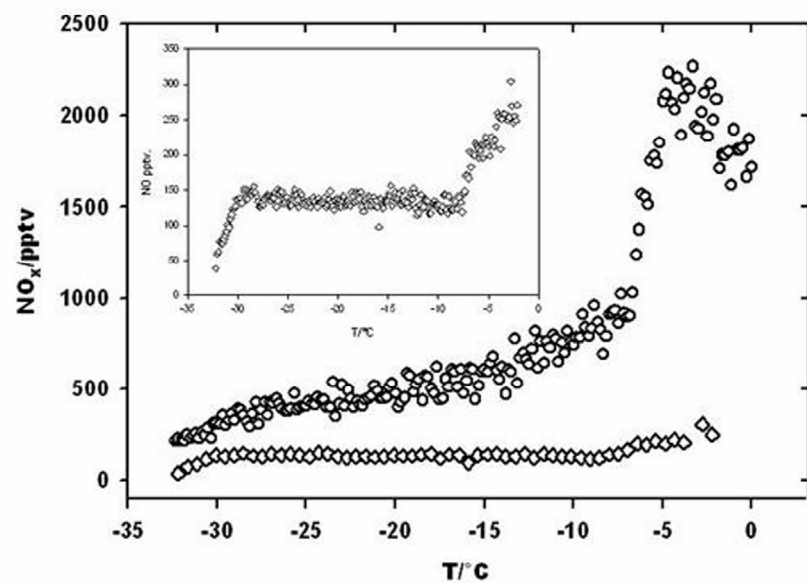


Figure 4.3a

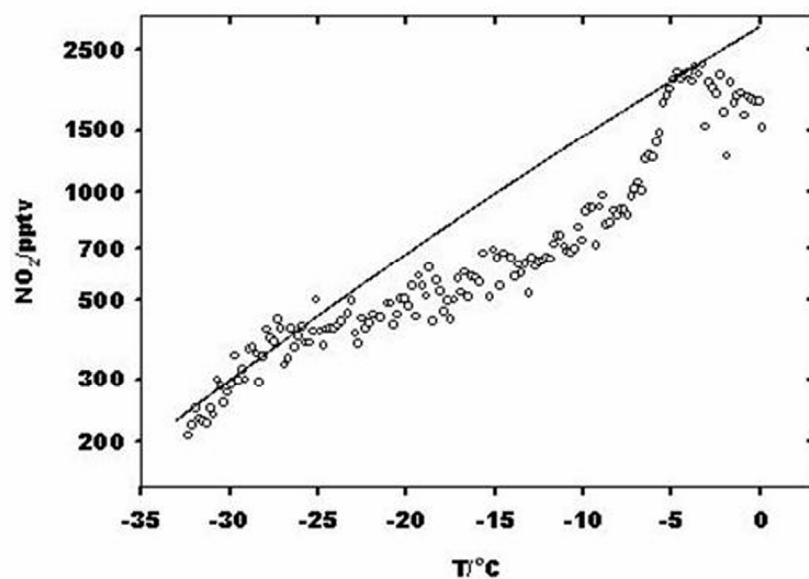


Figure 4.3b

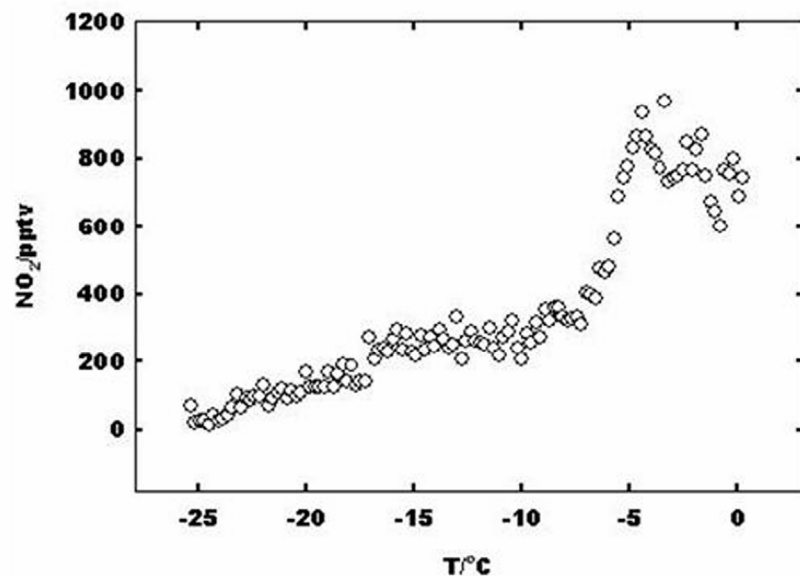


Figure 4.4

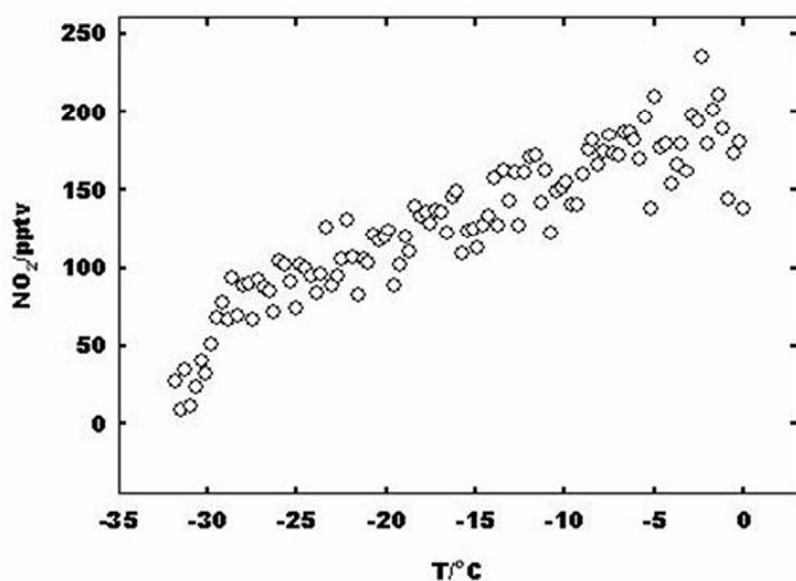


Figure 4.5

References

- (1) Legrand, M.; Mayewski, P. *Rev. Geophys.* **1997**, *35*, 219-243.
- (2) Wolff, E. W. *NATO ASI Ser.* **1995**, *I 30*, 195-224.
- (3) Dibb, J. E.; Arsenault, M.; Peterson, M. C.; Honrath, R. E. *Atmos. Environ.* **2002**, *36*, 2501-2511.
- (4) Davis, D.; Nowak, J. B.; Chen, G.; Buhr, M.; Arimoto, R.; Hogan, A.; Eisele, F.; Mauldin, L.; Tanner, D.; Shetter, R.; Lefer, B.; McMurry, P. *Geophys. Res. Lett.* **2001**, *28*, 3625-3628.
- (5) Honrath, R. E.; Peterson, M. C.; Guo, S.; Dibb, J. E.; Shepson, P. B.; Campbell, B. *Geophys. Res. Lett.* **1999**, *26*, 695-698.
- (6) Peterson, M. C.; Honrath, R. E. *Geophys. Res. Lett.* **2001**, *28*, 511-514.
- (7) Domine, F.; Shepson, P. B. *Science* **2002**, *297*, 1506-1510.
- (8) Dubowski, Y.; Colussi, A. J.; Hoffmann, M. R. *J. Phys. Chem. A* **2001**, *105*, 4928-4932.
- (9) Dubowski, Y.; Colussi, A. J.; Boxe, C.; Hoffmann, M. R. *J. Phys. Chem. A* **2002**, *106*, 6967-6971.
- (10) Ramamurthy, V.; Weiss, R. G.; Hammond, G. S. *Adv. Photochem.* **1993**, *18*, 67-234.
- (11) Trudinger, C. M.; Enting, I. G.; Etheridge, D. M.; Francey, R. J.; Levchenko, V. A.; Steele, L. P. *J. Geophys. Res.* **1997**, *102*, 6747-6763.
- (12) Maeno, N.; Ebinuma, T. *J. Phys. Chem.* **1983**, *87*, 4103-4110.
- (13) Hoyland, K. V. *Cold Regions Sci. Technol.* **2002**, *34*, 143-158.
- (14) Albert, M. R.; Grannas, A. M.; Bottenheim, J.; Shepson, P. B.; Perron, F. E. *Atmos. Environ.* **2002**, *36*, 2779-2787.

- (15) Sokratov, S. A. *Cold Regions Sci. Technol.* **2001**, *33*, 263-274.
- (16) Adams, E. E.; Miller, D. A.; Brown, R. L. *J. Appl. Phys.* **2001**, *90*, 5782-5785.
- (17) Mizuno, Y.; Wakahama, G. *J. Phys. Chem.* **1983**, *87*, 4161-4167.
- (18) Calvert, J.; Pitts, J. N. *Photochemistry*; Wiley: New York, 1966.
- (19) Sandholm, S.; Smyth, S.; Bai, R.; Bradshaw, J. *J. Geophys. Res.* **1997**, *102*, 28651-28661.
- (20) Honrath, R. E.; Guo, S.; Peterson, M. C.; Dziobak, M. P.; Dibb, J. E.; Arsenault, M. *A. J. Geophys. Res.* **2000**, *105*, 24183-24190.
- (21) Warneck, P.; Wurzinger, C. *J. Phys. Chem.* **1988**, *92*, 6278-6283.
- (22) Koenig, T.; Fischer, H. In *Free Radicals*; Kochi, J., Ed.; Wiley: New York, 1973; Vol. 1, chapt. 4.
- (23) Buxton, G. V.; Greenstock, C. L.; Helman, W. P.; Ross, A. B. *J. Phys. Chem. Ref. Data* **1988**, *17*, 513-886.
- (24) Wolff, E. W. *NATO ASI* **1996**, *I 43*, 541-559.
- (25) Rempel, A. W.; Waddington, E. D.; Wetzlaufer, J. S.; Worster, M. G. *Nature* **2001**, *411*, 568-571.
- (26) Gross, G. W.; McKee, C.; Wu, C. *J. Chem. Phys.* **1975**, *62*, 3080-3084.
- (27) Killawee, J. A.; Fairchild, I. J.; Tison, J. L.; Janssens, L.; Lorrain, R. *Geochim. Cosmochim. Acta* **1998**, *62*, 3637-3655.

- (28) Takenaka, N.; Ueda, A.; Daimon, T.; Bandow, H.; Dohmaru, T.; Maeda, Y. *J. Phys. Chem.* **1996**, *100*, 13874-13884.
- (29) Gross, G. W.; Gutjahr, A.; Caylor, K. *Journal De Physique* **1987**, *48*, 527-533.
- (30) Gross, G. W. *Adv. Chem. Series*, **1968**, *73*, 27-97.
- (31) Lodge, J. P.; Baker, M. L.; Pierrard, J. M. *J. Chem. Phys.* **1956**, *24*, 716-719.
- (32) Workman, E. J.; Reynolds, S. E. *Phys. Rev.* **1950**, *78*, 254-259.
- (33) Nye, J. F. *J. Glaciol.* **1989**, *35*, 17-22.
- (34) Cho, H.; Shepson, P. B.; Barrie, L. A.; Cowin, J. P.; Zaveri, R. *J. Phys. Chem. B* **2002**, *106*, 11226-11232.
- (35) Menzel, M. I.; Han, S. I.; Stapf, S.; Blumich, B. *J. Magn. Reson.* **2000**, *143*, 376-381.
- (36) Morse, P. M. *Thermal Physics*; 2nd ed.; Benjamin: New York, 1969.
- (37) Kallay, N.; Cakara, D. *J. Coll. Interfac. Sci.* **2000**, *232*, 81-85.
- (38) Hobbs, P. V. *Ice Physics*; Clarendon: Oxford, 1974.
- (39) Dash, J. G. *Rev. Mod. Phys.* **1999**, *71*, 1737-1743.
- (40) Dash, J. G.; Fu, H. Y.; Wetlaufer, J. S. *Rep. Prog. Phys.* **1995**, *58*, 115-167.
- (41) Fletcher, H. N. *Phil. Mag.* **1968**, *18*, 1287.
- (42) Fukazawa, H.; Sugiyama, K.; Shinji, M.; Narita, H.; Hondoh, T. *Geophys. Res. Lett.* **1998**, *25*, 2845-2848.
- (43) Israelachvili, J. *Intermolecular and Surface Forces*; 2nd ed.; Academic: London, 1992.
- (44) Wetlaufer, J. S. *Phys. Rev. Lett.* **1999**, *82*, 2516-2519.
- (45) Sadtchenko, V.; Ewing, G. E. *J. Chem. Phys.* **2002**, *116*, 4686-4697.
- (46) Doppenschmidt, A.; Butt, H. J. *Langmuir* **2000**, *16*, 6709-6714.

(47) Maeda, N.; Israelachvili, J. N.; Kohonen, M. M. *Proc. Nat. Acad. Sci. USA* **2003**,
100, 803-808.